Radioanatomical Study of the Rose-Ringed Parakeet (*Psittacula Krameri*) Head Based on the Findings of Computed Tomography Scanning

Siamak Alizadeh[a] Mohammadreza Hosseinchi[b] Raman Esmaeilnejad[c]

[a]Department of Veterinary Medicine, Faculty of Veterinary Medicine, Urmia Branch, Islamic Azad University, Urmia, Iran.

[b]Department of Basic Sciences, Faculty of Veterinary Medicine, Urmia Branch, Islamic Azad University, Urmia, Iran.

[c]Doctor of Veterinary Medicine, Faculty of Veterinary Medicine, Urmia Branch, Islamic Azad University, Urmia, Iran.

Corresponding author: Dr. Siamak Alizadeh

Postal address: Urmia. P.O. Box: 5715747774

University/organization email address: Si.Alizadeh@iau.ac.ir

ORCID ID: https://orcid.org/0000-0003-1112-7026

Tel. number: 09141891709

ABSTRACT

Computed tomography scanning is one of the most practical and precise diagnostic imaging methods that can be utilized to evaluate the head in birds. This study aimed to present the normal anatomical data of the head of the Rose-ringed parakeet (*Psittacula krameri*) using the CT method. In this research, the features of this bird's head were investigated in terms of bones, joints, muscles, sinuses, and other constituent tissues. The current retrospective cross-sectional study used carcasses of six adult Rose-ringed parakeet (3 males and 3 females) with an average age of 1–5 years and an average weight of 115–125 g. Following preparing the CT images, the head of each parrot underwent gross anatomy studies. Based on the results, reconstructed CT images could identify most structures of the Rose-ringed parakeet head. Parietal, mandible, occiput, maxillary, preimaxillary, palatine, pterygoid, quadrate, and temporal bones, epithelial membranes, external ear canal and bony labyrinth, ossicles and entoglossal bones, different parts of the infraorbital sinus, brain hemispheres, and various parts of the eyeball and conchae of the nasal cavities were examined in CT images. The results related to the CT evaluation and anatomical examination of the Rose-ringed parakeet's head demonstrated a high correlation. The results of this research can be employed for identifying anatomical features, examining different species of the Rose-ringed parakeets (*Psittacula krameri*), teaching anatomy, and interpreting CT scan images, as well as performing clinical examinations and treating this type of parrot.

Keywords

Computed tomography, Head, Radioanatomical, Rose-ringed parakeet (*Psittacula krameri*)

Abbreviation

CT: Computed Tomography

Introduction

Rose-ringed parakeet (*Psittacula krameri*), belongs to the family of green parrots (*Psittaculidae*) [1]. This parrot is also known as Halsbandsittich (German), Perruche à collier (French), or Cotorra de Kramer (Spanish) [2]. It is similar in appearance to the Alexandrine parakeet (*Psittacula eupatria*), but the king parrot (*Alisterus scapularis*) is slightly larger and has no red spots on the edges of its wings [3]. The body length of the Rose-ringed parakeets and their wingspan are typically around 40 cm and 15–17.5 cm, respectively. Their weight is between 115 and 130 g, and the size of the male parrot is slightly larger than that of the female. The average life span of these parrots in captivity is 20–30 years, and it has been reported to be more than 40 years in some cases. The heads of parrots are normally large and make up about 15–20% of the total body weight [4]. The eyes constitute the bulk of the skull and are placed inside a sclerotic pupil (Figure 1). In some parrot species, the lower part of the eye is surrounded by a unique bony arch or suborbital arch [5]. The rostrum of the parrot is connected to the skull bone by a joint, which gives the rostrum the ability to move upwards. The parrot's tongue is more active and agile due to the entoglossal bones inside the mouth [6]. The mandible and maxilla of these birds are placed inside the upper and lower elements of the beak [7]. The upper jaw contains the nasal cavity, inside which the turbinates, or conchae, are stretched longitudinally. Among the diagnostic imaging techniques, conchae can merely be detected with computed tomography [8]. Parrots have distinct sinuses on their faces. The primary sinus chamber and the infraorbital sinus surround the ventral part of the eyeball and then extend to areas around the eyes and ears through a series of canals. Some of these canals, along with the cervicocephalic air sac, extend to the central concha, the lower jaw, and the posterior parts of the neck. Except for the rostral part of the infraorbital sinus, these sinuses can be examined only through CT or magnetic resonance imaging (MRI) [9]. Parrots lack the prefrontal, postfrontal, temporal, and postparietal skull bones. The palatal bones of parrots are small and light. These birds lack teeth and have a large and ossified brain chamber, which leads to weight loss and ease of flight in these parrots [10, 11]. Parrots kept at home and able to fly may

suffer from head injuries under certain conditions. For instance, the bird may hit the window or land in an inappropriate place, which leads to traumatic injuries. Various imaging techniques can be beneficial in diagnosing these types of damage. Today, CT is one of the most accurate and practical diagnostic imaging methods that can be employed to evaluate head diseases in birds. Veladiano et al. (2016) examined the natural anatomy of the heads of blue-and-yellow macaws (*Ara ararauna*), African gray (*Psittacus erithacus*), and monks (*Myiopsitta monachus*) by CT, labeled different parts of their heads on CT images, and finally introduced the obtained findings as an atlas of the natural head anatomy of these parrots [12]. Faillace et al. (2021) investigated the anatomical features of the head of the blue-fronted Amazon parrot (*Amazona aestiva*) by the CT method. According to this research, some of these features, such as the size and position of the nasal conchae, the infraorbital sinus chamber, the nasopharyngeal duct, and the paraglossum, were different in this type of parrot compared to other parrots, which can be used in anatomy analysis [13]. They also reported that the inner ear and its related structures and the paratympanic sinus cannot be well-examined in normal CT images of this type of parrot. Thurber et al. (2015) evaluated the differential diagnosis of parrots' neurological symptoms caused by hydrocephalus syndrome. They concluded that CT is a suitable screening tool for diagnosing hydrocephalus in this type of sick bird [14]. In addition, using potassium iodide contrast medium and CT imaging, Jones et al. (2019) investigated the radioanatomical characteristics of the rock dove, or the common pigeon, especially in the head. They found that CT scanning can be utilized as a preferred method for examining different body tissues of this type of bird, and the images obtained with this method will be a valuable source for clinical applications and educational and research purposes [15]. Using CT, Duymus et al. (2013) compared the head anatomy of white, brown, and wild Japanese quails in terms of the head volume, brain volume, parietooccipital air space volume, and calvarial bone volume and indicated that the head of white quails had the lowest volume values, which was due to genetic differences [16]. Several studies have demonstrated the diagnostic value of CT in the diagnosis of complications and disorders of the head of parrot. Hébert (2019) confirmed

Rostroparasphenopalatal luxation in a red-crowned parakeet (*Cyanoramphus novaezelandiae*) by the CT method, and the bird completely recovered after therapeutic measures [17]. Krautwald-Junghanns et al. (1998) compared radiology and CT scan techniques in the diagnosis of head diseases in sick parrots and reported the superiority of the CT method in the diagnosis of complications such as fractures of the head bones and identification of hypercalcification or hypocalcification and carcinoma in this area [18]. The investigation of the tomographic features of the head of the Rose-ringed parakeet can be beneficial in identifying anatomical features and evaluating its pathological cases. However, a precise examination of details related to the normal anatomy (morphology and morphometry) of the different parts of this bird's head is necessary. Currently, radioanatomical studies of the head of the Rose-ringed parakeet are rare, and there are no detailed reports in this respect. Accordingly, this study aimed to investigate the normal anatomy of the Rose-ringed parakeet's head by CT using three-dimensional (3D) modeling. The CT evaluation and anatomical examination of a bird will simultaneously provide valuable findings in this regard. The results of this research can be used as a standard reference and atlas in identifying anatomical characteristics, investigating different species of Rose-ringed parakeets, teaching anatomical sciences, interpretation of CT scan images, and clinical examinations and treatment of this type of parrot.

Results

Based on the results, most structures of the head of the Rose-ringed parakeet (*Psittacula krameri*) were detectable by reconstructed CT images. In the 3D images, the head of this parrot was round and compact. The jugal arch and the palatine bone were fused in the remaining parts of the skull, except for the bones of the cranial parts of the face. Small bones of the head, such as ear bones and entoglossal bones inside the mouth, could also be evaluated in these CT images. In this research, it was possible to observe the bony trabecular in the head of this type of parrot by using the lung window. In addition, parietal and temporal bones, nasal conchae, epithelial membranes,

the external ear canal, and bony labyrinth were examined using this filter. Further, with covering tissues, different parts of the infraorbital sinus could be observed using this window. Furthermore, different soft tissue windows were adjusted to identify brain hemispheres, cerebellum, optic nerve, pupil muscles, and eye lenses (Figures 3-5). Based on the findings, the columella ossicle, its external cartilage, and the cochlea were undetectable in CT images. The eyeballs of all parrots were complete and bony and located on the skull's lateral side (Figure 3i). The mandible was bony and lacked a distinct symphysis (Figures 3b and 4a). The rostrum was keratinous, large, and curved ventrally. Moreover, the operculum could be identified in the dorsal part of the nostrils (the dorsal base of the nose). The occipital, maxillary, premaxillary, mandible, palatine, pterygoid, and quadrate bones were pneumonized and had air bubbles. The nasal cavities were separated by a septum. The thickness of this septum slightly increased from the rostral to the caudal side. The caudal third of this septum was cartilaginous, and the middle third and the rostral parts were bony. The ectethmoid, mesethmoid, maxillary, and preimaxillary bones were involved in the formation of the nasal cavity. The nasal cavity had olfactory, respiratory, and vestibular parts. Each nasal cavity had a single duct with caudal, middle, and rostral cartilaginous conchae. The rostral concha was C-shaped and located on the vestibular part of the nasal cavity. The thickness of this concha decreased from the rostral to the caudal direction. The rostral concha contained a basal lamella and was placed on the lateral wall of the nasal cavity. The middle concha was in the form of long ducts that originated from a basal lamella and was located in the upper respiratory tract of the nasal cavity. This lamella also splits into a sinusoidal lamella and a spiral lamella. This spiral lamella extended to the entrance of the nasopharyngeal canal. The caudal concha was small and hollow and was located in the caudal part of the nasal cavity. The nasal and oral cavities were connected through the nasopharyngeal canal (Figures 4c and 5h). The nasopharyngeal duct was connected to the maxilla-palatal process and the choanal part of the palatine bone from the rostrolateral and caudal sides, respectively. The caudal part of the nasopharyngeal duct was linked to the interorbital septum (Figures 4e and 5f). The oral cavity consisted of palatal, mandible, premaxillary, and

maxillary bones, as well as their related muscles and tongue. These oral bones, along with the pterygoid, also played a role in the formation of the pharynx (Figures 5c-d). The choana was located in the dorsal part of the pharynx and oral cavity and connected the oral cavity to the nasal cavity (Figure 3g). The strong and large tongue of the Rose-ringed parakeet (*Psittacula krameri*) could be identified in the CT images, which was located in the caudal and middle third of the inferior part of the oral cavity (Figures 3c-d). The oral cavity had a hyobranchial apparatus. The base of the tongue was in close contact with the paraglossum and the cranial part of the basihyal. Bishyal processes and uhorial bones were detectable in the trachea's larynx and cranial part. The branchial horn (the caudal part of the hyobranchial apparatus) was located in the inner part of the ramus of the mandible, or the cranial part of the trachea. The caudal third of the branchial horn was related to mandible masseter muscles. The larynx consisted of a ring-shaped cricoid cartilage and two pyramid-shaped arytenoid cartilages. The results of the current study demonstrated that the procricoid cartilage was located in the middle part of the cricoid cartilage and formed the dorsocaudal part of the larynx (Figures 3b-j). The glottis was located in the central part of the larynx and was surrounded by the arytenoid cartilages. Laryngeal mounds (Mons laryngealis) were detectable in cross-sectional CT images. The place where the cricoid joins the tracheal cartilages was found to be ring-shaped in these images Figures 3f and 5f).

The entire cavity of the pupil was filled with an oval eyeball. The frontal bone and the suborbital arch formed the outer edges of the eyeball. There was a trabecular bony septum between the pupils of the eye. All parrots under study had a complete bony eyeball (Figures 3j and 5h). In the obtained CT images, the eye lens was not clearly detectable, and the cranial chamber (aqueous) and the caudal (vitreous) were not distinguishable. The retina was unrecognizable. Eyeball muscles, lacrimal glands, and the third eyelid (nictitating membrane) had the same attenuation and could not be separated from each other. The scleral bones were found as two indistinct lines in cross-sectional images and circular or round in sagittal images (Figures 3j, 4a, and 5h).

The encephalon of the Rose-ringed parakeet (*Psittacula krameri*) could be evaluated in the CT images (Figures 4c and 5i). In the cadaver samples, brain hemispheres such as telencephalon and diencephalon, as well as the brainstem and cerebellum, were well detectable and could be distinguished from each other. However, these structures had similar attenuation in CT images, and their distinction was difficult. The findings revealed that the external acoustic meatus and the external opening of the ear of the Rose-ringed parakeet can be recognized in CT images (Figures 3m and 5c). Identifying the tympanic membrane in the CT images and carcasses of these birds was impossible. Hence, different parts of the middle ear were not distinguishable. Nonetheless, the presence of low-resolution lines in the distal third of the external acoustic meatus can demonstrate parts of the middle ear such as infraorbital (columella) and extracolumella cartilage. The bony labyrinth of the inner ear was well-recognized in the cadaver samples and CT images.

Based on our findings, the paratympanic sinus could not be detected in CT images. The muscles of the head were found as hyperattenuated lines and were not highly clear. Nonetheless, relatively larger muscles, such as quadrate, pterygoid, and ethmomandibular muscles, were somehow distinguishable. Although the jaw adductor muscle is large, it was not highly detectable in CT images (Figures 3g and 5c). The infraorbital sinus was surrounded by skull bones and covering and muscular tissues and was found as a large triangular cavity that covered a large part of the head. The premaxillary bone was located in the rostral part of this sinus. In addition, the palatine and pterygoid bones were located in its inner part. Further, the quadrate, jugal arch, and mandible bones were located in the lateral part. This sinus included the rostral diverticulum, transverse canal, postorbital, preorbital, infraorbital, quadrate bones, cervicocephalic diverticulum, and mandibular recess. The rostral diverticulum and the transverse canal were single, and the remaining parts were in pairs. Except for the periorbital parts, the transverse canal, and the rostral diverticulum, the remaining parts of the suborbital sinus were covered by the masticatory muscle (Figures 3-5). The rostral diverticulum extended along the preimaxillary bone. This diverticulum was divided into two parts by a narrow bony septum. The thickness of this septum decreased from

the rostral to the caudal direction, so it completely disappeared in the middle parts of the diverticulum. The transverse channel was visible as a short and horizontal channel. The maxillary process of the palatine bone and the upper jaw-palatine process (maxillopalatine) of the maxillary bone were located in this canal's ventral and distal parts, respectively. The transverse canal connected the periorbital region and rostral diverticulum (Figures 3a, 4d, and 5h). The nasopharyngeal duct divided the periorbital region into left and right parts. The jugal portion was connected dorsally with the periorbital region, ventrally with the choanal part of the palatine bone, and laterally with the jugal arch. A relatively thin epithelial layer separated the periorbital from the jugal portion. These subdivisions were connected in the caudal part and placed near the infraorbital part of the infraorbital sinus. The infraorbital part was the largest part of the infraorbital sinus. It covered a large area of the ventral surface of this sinus and extended to the eyeball. This part was connected to the palatine bone and interorbital septum from the medial part and to the suborbital and jugal arches from the lateral part. The infraorbital and postorbital parts were directly connected. The infraorbital and postorbital parts were the largest parts of the infraorbital sinus, respectively. The postorbital part was located in the pterygoid's lateral part, the zygomatic process's internal part, and the jugal bow's posterior part, which was connected with the musculature. The masseter, pterygoid, quadrate, and temporal muscles were located in the postorbital area. The caudoventral part of postorbital was connected to the quadrate portion. The smallest part of the infraorbital sinus was related to a quadrate part, which was laterally connected with the quadrate bone. The mandibular recess and cervicocephalic diverticulum were linked to the postorbital part. The mandibular recess was visible in the inner and rostral parts of the mandibular ramus. In fact, this recess was located in the inner part of the postorbital and the ventral part of the infraorbital canal. Based on the findings, the cervicocephalic diverticulum was detectable in the skull of the Rose-ringed parakeet (*Psittacula krameri*) and extended to the neck parts (Figures 3n and 4b).

Discussion

Based on CT and gross anatomy results, the skull of the Rose-ringed parakeet (*Psittacula krameri*) was similar to that of other parrots, and there was no difference between the skulls of male and female parrots. The CT diagnostic method enabled the anatomical description of the skull of the Rose-ringed parakeet (*Psittacula krameri*), which is in line with the reports of some researchers in this field [19, 20]. Although the heads of these types of parrots were small, the quality and clarity required to identify the bones and tissues of the head, such as the jugal arch, palatine bone, ear ossicles, and antoglossum bones inside the mouth and different parts of the infraorbital sinus, were provided in the obtained CT images. Of course, the type of CT scanner that was employed in this study (Toshiba Multi-slice CT scanner Asteion Premium 4, Model: TSX-021B, Japan) played an essential role in the quality and resolution of the obtained images, and this device obtained appropriate images of the heads of these parrots. In this research, the bony trabeculae of the head of the Rose-ringed parakeet were observed by using a suitable window (WW: 2336 HU; WL: 368 HU). Parietal and temporal bones, nasal conchae, epithelial membranes, external acoustic meatus, and bony labyrinth were identified as well. By performing head CT in the sagittal, transverse, and dorsal planes, were obtained images of different tissues of the head, especially various parts of the infraorbital sinus, were obtained, which had diagnostic value. Scanning the head in different planes solved the problem of superimposition of the images of different tissues, and each of the tissues was individually and specifically evaluated accordingly. Cubo and Casinos (2000) examined the bones of different species of birds and reported that some bones of birds contain air bubbles [21], which conforms to the results of our study. Based on our observations, some of the bones related to the skull of the Rose-ringed parakeet, such as the occipital, maxillary, preimaxillary, mandible, palatine, pterygoid, and quadrate bones, are trabecular and pneumonized and have air bubbles. In another study, Veladiano (2018) investigated the head CT of different birds and described the role of the pneumatic foramen, suborbital and paratympanic sinuses [22], which contradicts our observations. Based on CT images of the head

of the Rose-ringed parakeet (*Psittacula krameri*), the pneumatic foramen was undetectable, and the origin of pneumatization of the head bones could not be evaluated. Furthermore, the paratympanic sinus could not be detected in these images, which is probably due to the fusion of this sinus with middle ear tissues.

In this study, the tympanic membrane and different parts of the middle ear could not be detected in the CT images. However, the presence of low-resolution lines in the distal third of the external acoustic meatus can demonstrate parts of the middle ear, such as columella and extracolumella cartilage. These results corroborate those of Wild's study (2015) [23]. In this study, it has been reported that the cochlea, tympanic membrane, extracolumella cartilage, and columella of parrots are extremely small and thus cannot be observed in CT images. Nonetheless, it is suggested that other diagnostic imaging methods, such as micro-CT and MRI, be used to evaluate these parts.

Some studies have indicated the presence of three conchae in the nasal cavities of birds [24, 25], which is consistent with our study findings. The results of the current study revealed that each nasal cavity of the Rose-ringed parakeet (*Psittacula krameri*) consisted of a single meatus, which had caudal, middle, and rostral cartilaginous conchae. Nevertheless, some other studies reported two conchae in the Congo gray parrot (*Psittacus erithacus*) [26], the budgerigar (*Melopsittacus undulates*) [27], and the brown-eared nightingale (*Hysipetes amaurotis*) [28], or more than three conchae in the petrel (Pagodroma sp.) [29]. In the nostrils of the Rose-ringed parakeet, the middle and caudal turbinates had the largest and smallest sizes, respectively, which conforms to the results of studies conducted on parrots by Hanafy (2021) and Al-Rubaie and Kadhim (2023) [25, 30]. In the skull of the Rose-ringed parakeet (*Psittacula krameri*), similar to other parrots, there is a middle concha in the form of a long duct, which is located in the upper respiratory airway and originates from a basal lamella, which itself is divided into a sinus lamella and a spiral lamella. Moreover, in this type of bird, the caudal concha is small and hollow and is placed in the caudal nasal cavity. However, the results of some studies contradict our observations in this regard. Faillace et al.

(2021), examining the CT results of the nasal conchae of the blue-fronted Amazon parrot (*Amazona aestiva*), indicated that the middle concha is a narrow linear structure inside the rostral concha [13]. They further found that in this type of parrot, the caudal concha can have different sizes, so that the size of this concha is large in some of these birds, while it is extremely small in others. In a study, Madkour (2019) claimed that the nasal conchae of some bird species have bone tissue in addition to cartilaginous tissue [31]. This recent report does not match the result of our study because, according to our observations, the structure of the nasal conchae of the Rose-ringed parakeet was purely cartilaginous, and this finding was confirmed by the attenuation of the CT images of the head. In another study, Van Zeeland (2018) investigated the upper respiratory tracts of parrots and reported that the nasopharynx is the place where the nasal cavities connect to the throat, and adenoids and most of the lymph tissues are located in this region [32]. The reports of this study are somewhat in line with our gross anatomy results. The nasal and oral cavities were linked through the nasopharyngeal duct in the Rose-ringed parakeet (*Psittacula krameri*). Based on CT images, the nasopharyngeal duct was rostrolaterally and caudally connected to the maxilla-palatal process of the maxillary bone and the choanal part of the palatine bone, respectively. The caudal part of the nasopharyngeal duct was linked to the interorbital septum. Unfortunately, it was impossible to find valid studies on the nasopharyngeal CT characteristics of birds and then compare their results with those of this study. It is hoped that the findings of this research pave the way for future research in this respect.

The oral cavity of the Rose-ringed parakeet (*Psittacula krameri*) had a hyobranchial apparatus. The caudal part of this system was located in the inner part of the mandible ramus, in other words, cranial part of trachea. These findings conform to the results of other studies performed on parrots. According to our observations, the base of the tongue was in close contact with the paraglossum and the cranial part of basihyal.

The results of the present study demonstrated that the pupil of the Rose-ringed parakeet (*Psittacula krameri*) is completely bony. In the gross anatomy studies, it was possible to determine

the anterior and caudal chambers, lens, and optic nerve of this bird's eye, which matches the reports of most researchers, and it seems that the eye anatomy of this type of parrot does not particularly differ from that of other birds [33]. However, unlike the gross anatomical evaluations, the lens was not clearly visible, and it was impossible to distinguish the ocular chambers in the obtained CT images. The retina was also unrecognizable. The muscles of the eyeball, lacrimal glands, and third eyelid (nictitating membrane) had the same attenuation and therefore could not be separated from each other. The researchers of this study could not find written and specific reports about CT scans of birds' eyes and compare them with the results of this study. However, according to the findings of this study, it is suggested that diagnostic imaging methods such as ultrasonography, micro-CT, MRI, and other specialized eye evaluation methods be used to examine the internal tissues of the eye.

In the CT images obtained from the head of this type of parrot, the masticatory muscle could be identified due to its large size. However, other head muscles, eyeball muscles, and even nerve vessels had highly close attenuation, and it was difficult to distinguish between them; thus, they did not undergo separate investigations. Different radiation factors were employed to increase the clarity and contrast of these tissues, but no suitable answer was obtained in this regard.

Based on anatomical examination of the budgerigar and Casco (African grey parrot), Smallwood (2014) reported that the cricoid cartilage of the larynx of these birds is wide and has a rostral process [34]. In another study, Silva et al. (2020) found that the cricoid cartilage of the larynx of the cockatiel is smooth and small and has two rostral and lateral processes [35], which contradicts our findings. In the Rose-ringed parakeet (*Psittacula krameri*), the larynx consisted of an annular cricoid cartilage and two pyramidal arytenoid cartilages. The cricoid cartilage was smooth and thin and had no processes. In the middle part of the cricoid cartilage, there was the procricoid cartilage, which formed the dorsocaudal part of the larynx.

In some previous studies, the anatomy of the infraorbital sinus has been described in some domestic birds such as hens, turkeys, and geese [36]. However, there is no detailed and

comprehensive report about the anatomy and CT features of the infraorbital sinus in parrots. Based on the findings of our study, the infraorbital sinus of the Rose-ringed parakeet (*Psittacula krameri*) was surrounded by skull bones and covering and muscular tissues, and in the CT images, it was detected as a large triangular cavity that covered a large part of the head. The premaxillary bone was located in the rostral part of this sinus. In addition, the palatine and pterygoid bones were located in its inner part, and the quadrate bone, jugal arch, and mandible bones were located in the lateral part. Grist (2006) conducted an anatomical study on domestic chickens and found that there were fewer infraorbital sinus chambers in the head of this type of bird [37]. The names and characteristics of these chambers were not mentioned in this report. Eventually, it was indicated that this sinus is shorter in other birds and is limited by the infraorbital part. According to our observations, this sinus included the rostral diverticulum, transverse canal, postorbital, preorbital, infraorbital, and quadrate parts, cervicocephalic diverticulum, and mandibular recess in the Rose-ringed parakeet (*Psittacula krameri*). The head and neck of this type of parrot were widely pneumatized with this sinus. No specific homologies were inferred in this regard since the analogy of the infraorbital sinus and phylogenetic evaluations between the Rose-ringed parakeet (*Psittacula krameri*) and other parrots was impossible.

Massari et al. (2020) performed CT on the head of a macaw and concluded that the infraorbital, periorbital, and rostral diverticulum of the infraorbital sinus can be easily detected, which is mainly due to the large chambers of this sinus and the absence of covering muscles in this region [38]. It was further indicated that the postorbital, quadrate, and mandibular recess parts were not detectable because they were small and superimposed by the masticatory muscle. These findings somewhat corroborate the results of our study. The findings of the present research revealed that in the Rose-ringed parakeet (*Psittacula krameri*), except for the periorbital, transverse canal, and rostral diverticulum, the remaining parts of the suborbital sinus were covered by the masticatory muscle.

In some studies, the existence of a paratracheal recess was reported in Amazon and Cockatoo [39], as well as Anodorhynchus and Ararauna macaws [40]. The results of these studies contradict

the findings of our research. Based on our observations, paratracheal recess was not observed in any of the Rose-ringed parakeets under investigation; therefore, this feature can be mentioned in the comparative anatomy of this type of parrot.

The skull of the Rose-ringed parakeet (*Psittacula krameri*) was relatively small, and the limit distance of its constituent bones was visible. The periorbital sinus was located in the anterorbital fenestra, and the zygomatic process of the squamosal bone surrounded the postorbital sinus. In the CT images, the muscles of the head of this parrot were detected as hyperattenuated lines and were not very clear. However, relatively larger muscles such as quadrate, pterygoid, and ethmomandibular muscles were somehow distinguishable. Although the jaw adductor muscle was large, it could not be detected in the CT images, and its boundaries was determined based on the topography of the bones in that region.

Based on the current study, the columella ossicle, its external cartilage, and the cochlea were not recognizable in CT images. This is mainly due to the small size of these structures. Hence, it is recommended that other diagnostic imaging methods such as micro-CT or MRI be utilized in cases where it is intended to evaluate these structures.

The analysis of the findings and their comparison with the results of other studies revealed that the skull of the Rose-ringed parakeet (*Psittacula krameri*) was not that much different from that of other parrots. The only morphological differences were related to some parts of the nasal cavity, the infraorbital sinus, and, to some extent, the hyobranchial apparatus and nasopharyngeal duct. In conclusion, the CT scan is one of the most appropriate and valuable diagnostic imaging methods to describe and dissect most of the hard and soft tissues of the head of the Rose-ringed parakeet (*Psittacula krameri*). The results of this study demonstrated that CT images can be used to examine the infraorbital sinus and the turbinates, or conchae, of nasal cavities. The investigation of the tomographic features of the head of the Rose-ringed parakeet (*Psittacula krameri*) can be useful in identifying anatomical features and evaluating its pathological cases. This study investigated the normal anatomy of the Rose-ringed parakeet's head by CT using 3D modeling. The

simultaneous study of CT evaluation and anatomical examination of the head of the Rose-ringed parakeet represented highly correlated findings. The results of this research can be utilized as a standard reference and atlas for identifying anatomical characteristics, examining various species of Rose-ringed parakeets (*Psittacula krameri*), teaching anatomy, and interpreting CT scan images. Moreover, they can be used for clinical examinations and treatment of this type of parrot.

Materials and methods

Ethical consideration

This work involved the use of procedures that did not differ from established internationally recognized high standards (best practice) of veterinary clinical care for the individual animals. The study was registered under registration code Ir.iau.urmia.rec.1403.038 in Ethical Committee of Islamic Azad University, Urmia.

Study plan and birds

The current retrospective cross-sectional study used carcasses of six adult Rose-ringed parakeets (*Psittacula krameri*) (3 males and 3 females) with an average age of 1–5 years and an average weight of 115–125 g, which were well-fed during their lifetime. The carcasses were obtained from a private breeding center for Rose-ringed parakeet in Tehran and then frozen and stored at -20°C. The parrots, which previously died for various reasons, were used in this study, and the cause of their deaths was unrelated to this study. The maturity of these parrots was confirmed based on factors such as the type of color of the neck ring, the amount of scales on the feet, the condition of the feathers, and the color of the beak. The sex of the parrot was also determined following a necropsy of the carcass [41, 42].

Computed tomography studies

To prepare CT images, the Rose-ringed parakeet was placed on the CT scan table in a sternal recumbent position, and the head of the bird was kept facing forward so that its mandible was perpendicular to the gantry. Head scans were performed in the sagittal, transverse, and dorsal

planes with a thickness and interval of 1 mm. A helical scanner (Toshiba Multi-slice CT Scanner Asteion Premium 4, Model: TSX-021B, Japan) was employed for CT. In addition, appropriate windows were selected to examine soft and bone tissues. The technical factors of the CT scanner included gantry rotation time (400 ms), slice thickness (1 mm), reconstruction distance (0.5–1 mm), pitch ratio (1), kVp (120), mAs (10), physical detector collimation (32 × 0.6 mm), final section collimation (64 × 0.6 mm), resolution (512 × 512 pixels), and resolution range (0.92 × 0.92), Kernel (10 H), and increment (0.5 mm) [13, 43]. Imaging was performed based on the above-mentioned factors, and the obtained images were saved in DICOM format) [44].

Three-dimensional reconstruction

After saving the obtained images in DICOM format, they were transferred to a computer loaded with 3D modeling software (Onis CT software, Multi-Modality Workplace: VE 2.5A) and displayed using bone window settings (window width: UH 4500 and window level: UH750), according to previous research [45]. Next, these images were analyzed with 3D slicer software [46]. Based on our observations, this technique allowed the use of lung (WW: 2336 HU; WL: 368 HU) and bone (WW: 950; WL: 390) windows, thus providing high-resolution images of the tissues and structures that constitute the head of parrots.

Anatomical studies

Following preparing CT images, the head of each of the frozen parrots was transversely cut with an electric band saw at intervals of 5 mm from the rostral part of the rhamphotheca to the anterior end of the neck. Each prepared slice was cleansed with water and a soft brush and photographed. Visible textures and structures were identified and labeled on these photographs. Further, CT images were matched with these photos and labeled accordingly. Nomina Anatomica Veterinaria was used as the obtained scientific term [47] (Figure 2).

References

1. Abed SA, Salim MA, Alsaffah SM. First record of Alexandrine Parakeet psittacula eupatria (Psittaculidae, psittaciformes)(Linnaeus 1766) in Iraq. Indian Journal of Ecology. 2020;47(3):887-8.
2. Braun M. Die Bestandssituation des Halsbandsittichs Psittacula krameri in der Rhein-Neckar-Region (Baden-Württemberg, Rheinland-Pfalz, Hessen), 1962-2008, im Kontext der gesamteuropäischen Verbreitung. Vogelwelt. 2009;130:77-89.
3. Şahin D, Arslangündoğdu Z. Breeding status and nest charactheristics of roseriged (Psittacula krameri) and alexandrine parakeets (Psittacula eupatria) in Istanbul's city park. Applied Ecology & Environmental Research. 2019;17(2). DOI: 10.15666/aeer/1702_24612471
4. Mentil L, Monti P, Fraticelli F, Carpaneto GM. A morphometric sexing approach for the Ring-necked Parakeet Psittacula krameri in Italy. Ringing & Migration. 2018;33(2):64-7. DOI: 10.1080/03078698.2018.1631609
5. Henley E. A bird's eye view of breakdown in parrot–caregiver relations. Companion Animal. 2018;23(2):104-8. DOI: 10.12968/coan.2018.23.2.104
6. Benedict L, Charles A, Brockington A, Dahlin CR. A survey of vocal mimicry in companion parrots. Scientific Reports. 2022;12(1):20271. DOI: 10.1038/s41598-022-24335-x
7. Forouzan P, Cohen PR. Parrot Beak nail: case report and review of parrot beak nail dystrophy. Cureus. 2021;13(6). DOI: 10.7759/cureus.15974
8. Langlois I, Barrs VR, Dufresne PJ. Corrigendum to 'Rhinitis due to Aspergillus pseudoviridinutans in an orange-winged Amazon parrot (Amazona amazonica)'[Med. Mycol. Case Rep. 30 (2020) 46–50]. Medical Mycology Case Reports. 2021;33(4):38-55 DOI: 10.1016/j.mmcr.2020.11.001
9. Faux CM, Logsdon ML. Infraorbital sinusitis. Comparative Veterinary Anatomy: Elsevier; 2022;11(2):1264-70.

10. Hollwarth AJ, Esmans MC, Herrmann A, Dutton TA. Heterotopic Ossification Bone Formation in the Frontal Bones of an African Grey Parrot (Psittacus erithacus). Journal of Avian Medicine and Surgery. 2023;36(4):388-93. DOI: 10.1647/22-00002
11. Carril J, Tambussi CP, Degrange FJ, Benitez Saldivar MJ, Picasso MBJ. Comparative brain morphology of Neotropical parrots (Aves, Psittaciformes) inferred from virtual 3D endocasts. Journal of anatomy. 2016;229(2):239-51. DOI: 10.1111/joa.12325
12. Veladiano IA. Tomographic imaging in companion avian species. 2018;13(2):655-666.
13. Faillace ACL, Vieira KRA, Santana MIS. Computed tomographic and gross anatomy of the head of the blue-fronted Amazon parrot (Amazona aestiva). Anatomia, Histologia, Embryologia. 2021;50(1):192-205. DOI: 10.1111/ahe.12618
14. Thurber MI, Mans C, Fazio C, Waller K, Rylander H, Pinkerton ME. Antemortem diagnosis of hydrocephalus in two Congo African grey parrots (Psittacus erithacus erithacus) by means of computed tomography. Journal of the American Veterinary Medical Association. 2015;246(7):770-6. DOI: 10.2460/javma.246.7.770
15. Jones ME, Button DJ, Barrett PM, Porro LB. Digital dissection of the head of the rock dove (Columba livia) using contrast-enhanced computed tomography. Zoological letters. 2019;5:1-31. DOI: 10.1186/s40851-019-0129-z
16. Duymus M, Demiraslan Y, Akbulut Y, Orman G, Ozcan S. The statistical analysis of some volumetric measurements in the japanese quails' head with different feather color: a computed tomography study. Kafkas Universitesi Veteriner Fakultesi Dergisi. 2013;19(4): 681-6. DOI: 10.9775/kvfd.2013.8650
17. Hébert JA. Closed Reduction of a Rostroparasphenopalatal Luxation in a Red-crowned Parakeet (Cyanoramphus novaezelandiae). Journal of avian medicine and surgery. 2019;33(3):285-8. DOI: 1082-6742-33.3.285

18. Krautwald-Junghanns M-E, Kostka VM, Dörsch B. Comparative studies on the diagnostic value of conventional radiography and computed tomography in evaluating the heads of psittacine and raptorial birds. Journal of Avian Medicine and Surgery. 1998;149-57.
19. Sabat D, Millan S, Suchismita Sethy P, Marathe S, Sahoo H, Mishra M, editors. Elemental analysis of various feathers of Indian Rose Ringed Parakeet Psittacula krameri. Acta Biology. 2017;14(3):47-66. DOI: 10.1007/978-3-319-46601-9_5
20. Iwaniuk AN, Dean KM, Nelson JE. Interspecific allometry of the brain and brain regions in parrots (Psittaciformes): comparisons with other birds and primates. Brain Behav Evol. 2004;65(1):40-59. DOI: 10.1159/000081110
21. Cubo J, Casinos A. Incidence and mechanical significance of pneumatization in the long bones of birds. Zoological Journal of the Linnean Society. 2000;130(4):499-510. DOI: 10.1111/j.1096-3642.2000.tb02198.x
22. Veladiano IA, Banzato T, Bellini L, Montani A, Catania S, Zotti A. Computed tomographic anatomy of the heads of blue-and-gold macaws (Ara ararauna), African grey parrots (Psittacus erithacus), and monk parakeets (Myiopsitta monachus). American journal of veterinary research. 2016;77(12):1346-56. DOI: 10.2460/ajvr.77.12.1346
23. Wild JM. The avian somatosensory system: a comparative view. Sturkie's Avian physiology. Elsevier. 2015;11(1):55-69. DOI: 10.1016/B978-0-12-407160-5.00005-1
24. Langlois I, Barrs VR, Dufresne PJ. Rhinitis due to Aspergillus pseudoviridinutans in an orange-winged Amazon parrot (Amazona amazonica). Medical mycology case reports. 2020;30:46-50. DOI: 10.1016/j.mmcr.2020.11.001
25. Hanafy BG. Structural adaption of the nasal conchae of Eurasian common moorhen (Gallinula chloropus chloropus, Linnaeus, 1758)—Histomorphological study. Microsc Res Tech. 2021;84(9):2195-202. DOI: 10.1002/jemt.23778
26. Pohlmeyer K, Kummerfeld N. Morphologie der Nasenhöhle und der nasen Nebenhöhlen sowie ihre klinische Bedeutung bei Grosspapageien. Kleintierpraxis. 1989;34:127-33.

27. Orosz S. Clinical respiratory anatomy. CABI Digital Library. 2016;247-53.
28. Yokosuka M, Hagiwara A, Saito TR, Aoyama M, Ichikawa M, Sugita S. Morphological and histochemical study of the nasal cavity and fused olfactory bulb of the brown-eared bulbul, Hysipetes amaurotis. Zoological science. 2009;26(10):713-21. DOI: 10.2108/zsj.26.713
29. Piro A, Acosta Hospitaleche C. Skull anatomy of Wilson's storm-petrel Oceanites oceanicus (Hydrobatidae, Procellariiformes). Polar Biology. 2019;42(8):1501-10. DOI: 10.1007/s00300-019-02536-x
30. Al-Rubaie NI and Kadhim, K. Anatomical Comparison of the Nasal Cavity in Adult Male and Female Cockatiel (Nymphicus Hollandicus). Acta Biology. 2023;94(3): 2023719.
31. Madkour F. Anatomical descriptions of the nasal cavity of the Aquatic and Non-aquatic birds. SVU-International Journal of Veterinary Sciences. 2019;2(2):101-10. DOI: 10.21608/svu.2019.14982
32. Van Zeeland Y. Upper respiratory tract disease. BSAVA Manual of Avian Practice: BSAVA Library; 2018;299-316. DOI: 10.22233/9781910443323.20
33. Moore BA, Oriá AP, Montiani-Ferreira F. Ophthalmology of psittaciformes: parrots and relatives. Wild and Exotic Animal Ophthalmology: Volume 1: Invertebrates, Fishes, Amphibians, Reptiles, and Birds. Springer. 2022; 3(12):349-91. DOI: 10.1007/978-3-030-71302-7_17
34. Smallwood JE. A Guided Tour of Avian Anatomy. Millennium Pring Group. 2014;155-167.
35. Silva IA, Vieira LC, Mancini VRM, Faillace ACL, Santana MIS. Radiographic anatomy of the cockatiel (Nymphicus hollandicus) axial and appendicular skeleton. Anatomia, histologia, embryologia. 2020;49(2):184-95. DOI: 10.1111/ahe.12510
36. Casteleyn C, Cornillie P, Van Cruchten S, Van den Broeck W, Van Ginneken C, Simoens P. Anatomy of the upper respiratory tract in domestic birds, with emphasis on vocalization. Anatomia, histologia, embryologia. 2018;47(2):100-9. DOI: 10.1111/ahe.12336

37. Grist A. Poultry inspection: anatomy, physiology and disease conditions. CABI Digital Library. 2006;276-292.

38. Massari CHdAL, Silva AF, Magalhães HIR, Silva DRS, Sasahara THdC, Miglino MA. Anatomía Comparada de los Picos de Guacamayo Azul y Amarillo (Ara ararauna) y de Tucán Toco (Ramphastos toco). International Journal of Morphology. 2020;38(6):1591-6. DOI: 10.4067/S0717-95022020000601591

39. Carril J, Tambussi CP, Rasskin-Gutman D. The network ontogeny of the parrot: Altriciality, dynamic skeletal assemblages, and the avian body plan. Evolutionary Biology. 2021;48:41-53. DOI: 10.1007/s11692-020-09522-w

40. Monção-Silva RM, Ofri R, Raposo ACS, Libório FA, Estrela-Lima A, Oriá AP. Ophthalmic parameters of Blue-and-yellow Macaws (Ara ararauna) and Lear's Macaws (Anodorhynchus leari). Avian Biology Research. 2016;9(4):240-9. DOI: 10.3184/175815516X14725499175746

41. Webb TJ, Gaston KJ. Geographic range size and evolutionary age in birds. Proc R Soc Lond B Biol Sci. 2000;267(1455):1843-50. DOI: 10.1098/rspb.2000.1219

42. Vučićević M, Stevanović J, Šekler M, Resanović R, Stanimirović Z. Historical overview of methods for sex determination in birds. Veterinarski glasnik. 2016; 11(2):145-57. DOI: 10.2298/VETGL1604145V

43. Ma S, Wang L, Liu Z, Luo X, Zhou Z, Xie J, et al. “One stone, two birds”: engineering 2-D ultrathin heterostructure nanosheet BiNS@ NaLnF 4 for dual-modal computed tomography/magnetic resonance imaging guided, photonic synergetic theranostics. Nanoscale. 2021;13(1):185-94. DOI: 10.1039/d0nr07590f

44. Brühschwein A, Klever J, Wilkinson T, Meyer-Lindenberg A. DICOM standard conformance in veterinary medicine in Germany: A survey of imaging studies in referral cases. Journal of Digital Imaging. 2018;31:13-8. DOI: 10.1007/s10278-017-9998-x

45. Wilhite R, Wölfel I. 3D Printing for veterinary anatomy: An overview. Anatomia, histologia, embryologia. 2019;48(6):609-20. DOI: 10.1111/ahe.12502

46. Šljivic M, Pavlovic A, Kraišnik M, Ilić J, editors. Comparing the accuracy of 3D slicer software in printed enduse parts. IOP conference series: materials science and engineering. IOP Publishing. 2019;12(1):100-119. DOI: 10.1088/1757-899X/659/1/012082

47. Constantinescu GM, Constantinescu IA. The updated international veterinary anatomical and embryological nomenclatures. Journal of Veterinary Science and Animal Husbandry. 2013;1(2):1-3. DOI: 10.15744/2348-9790.1.e201

Figure Legends

Figure 1. Rose-ringed parakeet (*Psittacula krameri*)

Figure 2. Representative photographs of anatomic cross sections of the adult cockatiel (Nymphicus hollandicus) head. A (level of the Eye) and B (level of the external acoustic meatus) in the dorsal plane and C (level of the rostral border of the orbital fossa) and D (level of the external acoustic meatus) in the transverse plane. **A**: (1) Ramphoteca, (2) Premaxilla bone, (3) Maxilla bone, (4) Left nasal cavity, (5) Caudal nasal concha, (6) Infraorbital sinus, (7) Eye, (8) Brain hemispheres, (9) Falx cerebri, (10) Occipital bone, (11) Temporal bone. **B**: (1) Ramphoteca, (2) Premaxilla bone, (3) Palatine bone, (4) Ethmomandibularis muscle, (5) Pterygoideus muscle, (6) Cerebellum, (7) Bony labyrinth, (8) External acoustic meatus, (9) Caudal nasal concha, (10) Occipital bone. **C**: (1) Fronto-parietal bone, (2) Eye, (3) Infraoebital sinus, (4) Pterygoideus muscle, (5) Ethmomandibularis muscle, (6) Hard Palate, (7) Eye, (8) Caudal nasal concha, (9) Lingual process of hyoid bone, (10) tongue, (11) Choanal cleft, (12) Mandible. **D**: (1) Cerebrum, (2) Falx cerebri, (3) Occipital bone, (4) Brain stem, (5) Chiasma optic, (6) External acoustic meatus, (7) Ethmomandibularis muscle, (8) Pterygoideus muscle, (9) Mandible, (10) Hard palate, (11) Lingual process of hyoid bone. R, Right; L, Left.

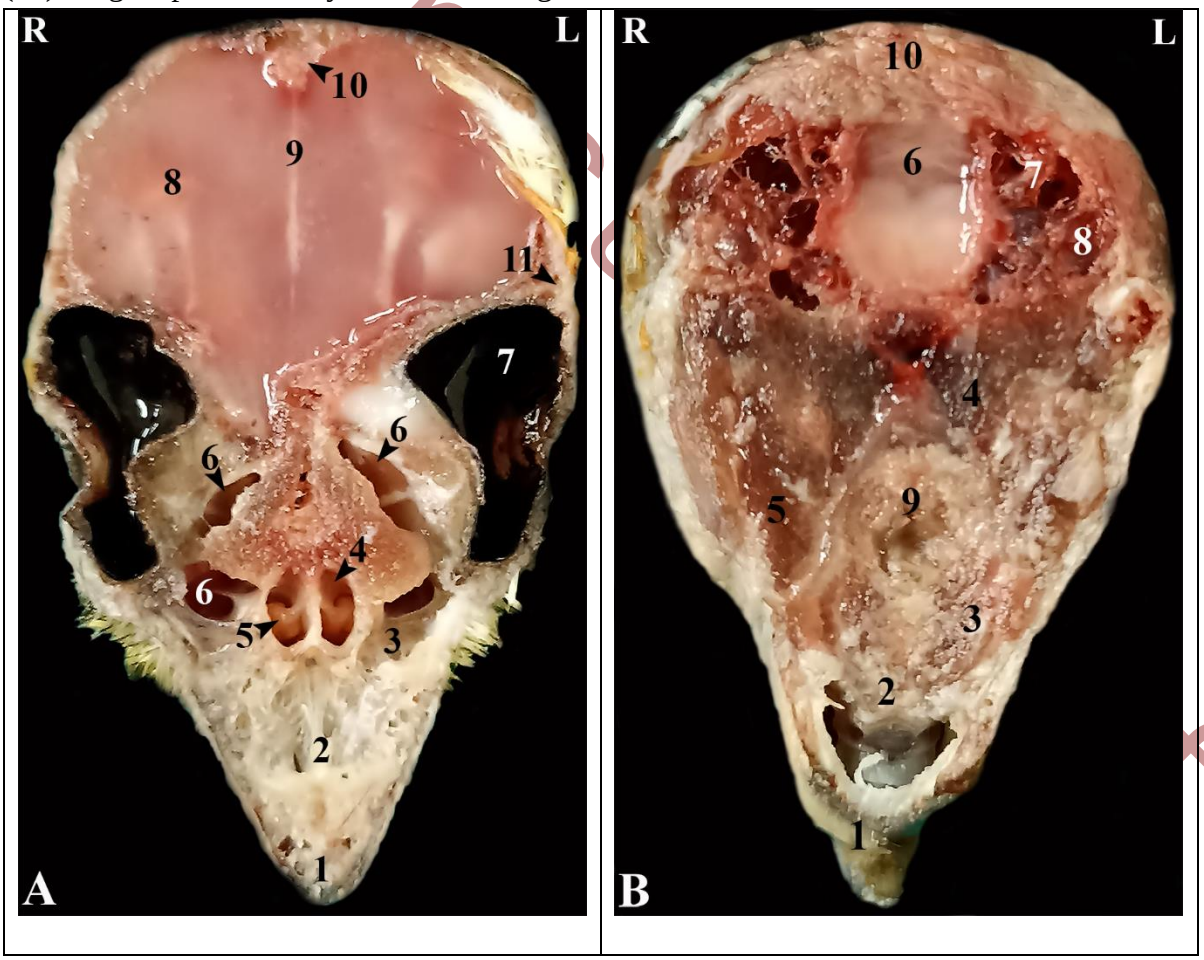

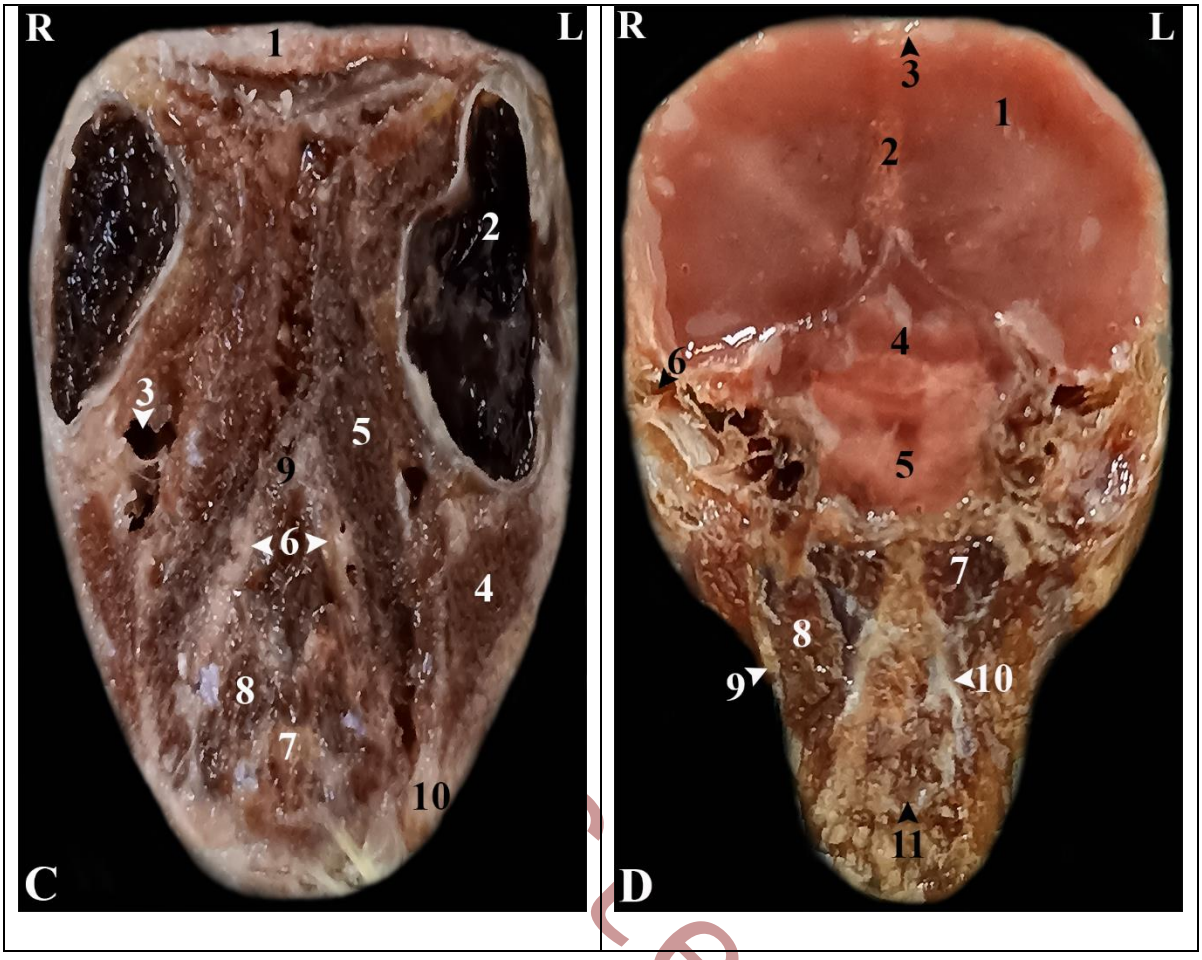

Figure 3. (a-n) Transverse computed tomography reconstruction images in the lateral plane of the normal skull of the cockatiel (*Nymphicus hollandicus*). (1) Rostral diverticulum septum, (2) Premaxillary bone, (3) Rostral diverticulum, (4) Paraglossum, (5) Bony part of nasal septum, (6) Mandible bone (pneumonized), (7) Palate bone opening, (8) Rostral nasal concha, (9) Transverse canal, (10) Maxillary process of palatal bone, (11) Tongue, (12) Middle nasal turbinate, (13) Basal layer of middle nasal turbinate, (14) Nasal cavity, (15) Cartilaginous part of nasal septum, (16) Nasopharyngeal airway, (17) Lateral border of palatine bone, (18) Periorbital process of infraorbital sinus, (19) Jugal part of infraorbital sinus, (20) Jugal arch, (21) Glottis, (22) Laryngeal protrusion, (23) Arytenoid cartilages, (24) Bronchial horn, (25) Trachea, (26) Choana of palatal bone, (27) Ethmomandibular muscle, (28) Periorbital part of the infraorbital sinus, (29) Caudal nasal turbinate, (30) Infraorbital sinus foramen, (31) Infraorbital part of the infraorbital sinus, (32) Eyeball, (33) Epithelial membrane, (34) Tracheal cartilage ring, (35) Infraorbital septum, (36) Cricoid cartilage, (37) Procricoid cartilage, (38) Scleral ossicles, (39) Suborbital arch, (40) Frontal bone (pneumonized), (41) Pterygoid and quadrate muscles, (42) Larynx, (43) Zygomatic process of the squamosal bone, (44) Quadrate bone (pneumatized), (45) Quadrature part of infraorbital sinus, (46) Postorbital part of infraorbital sinus, (47) External acoustic meatus, (48) Cervicocephalic diverticulum, (49) Brain stem, (50) Bony labyrinth. L, Left; R, Right.

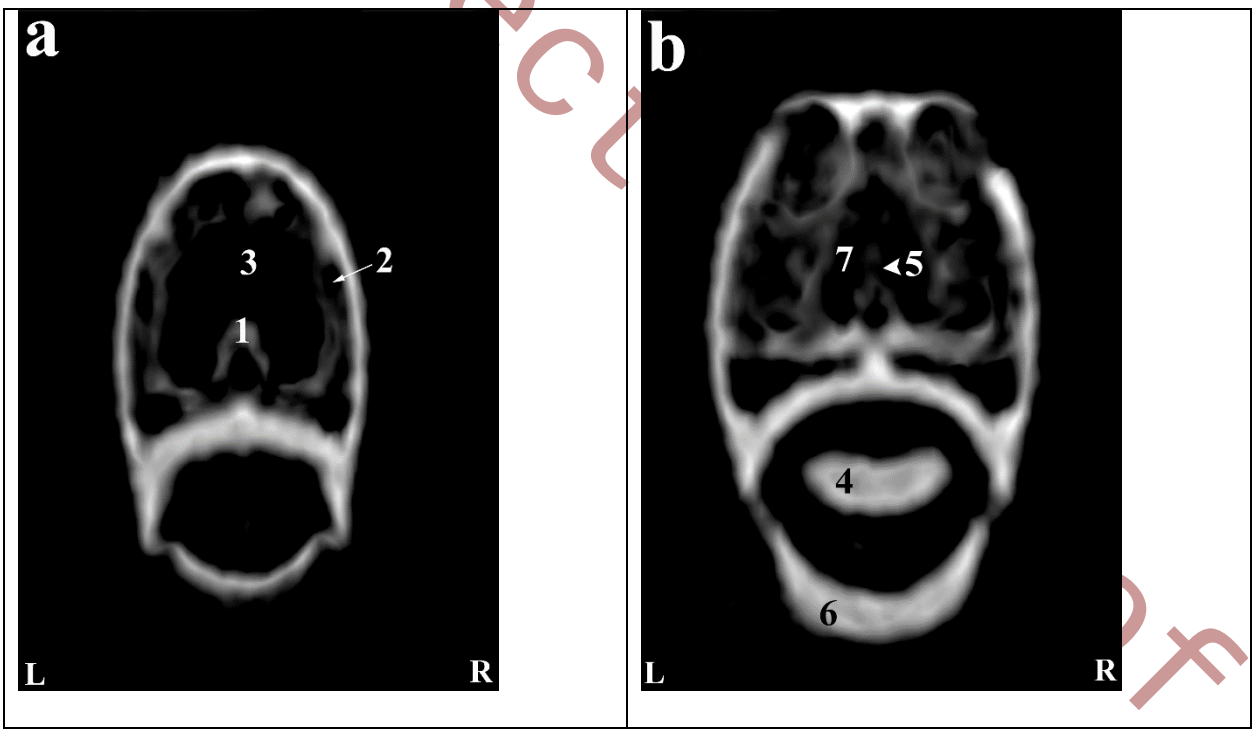

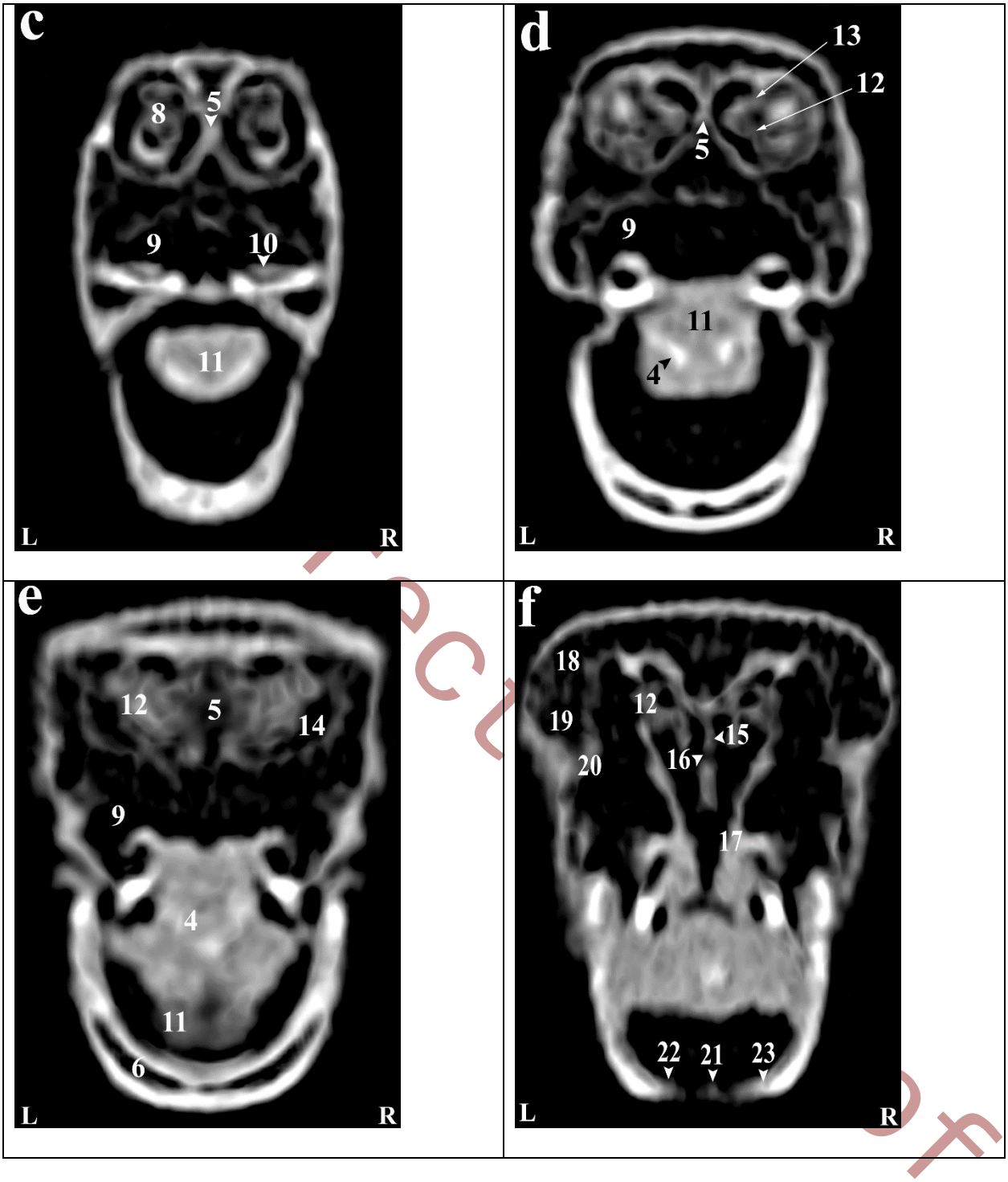
c
8
5
9
10
11
L
R
d
13
12
5
9
11
4
L
R
e
12
5
14
9
4
11
6
L
R
f
18
19
12
15
20
16
17
22
21
23
L
R

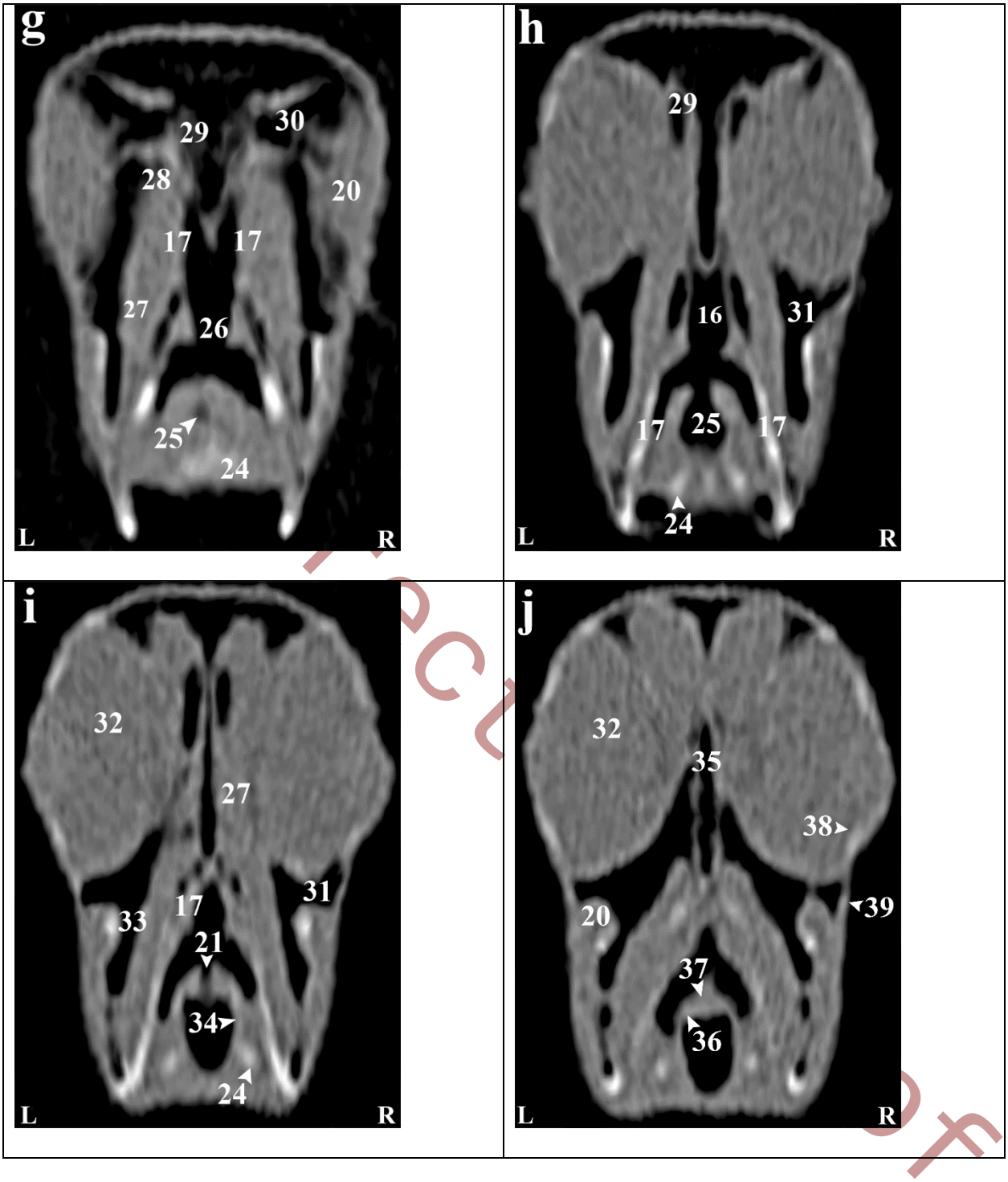
g
29
30
28
20
17
17
27
26
25
24
L
R
h
29
16
31
17
25
17
24
L
R
i
32
27
31
17
33
21
34
24
L
R
j
32
35
38
39
20
37
36
L
R

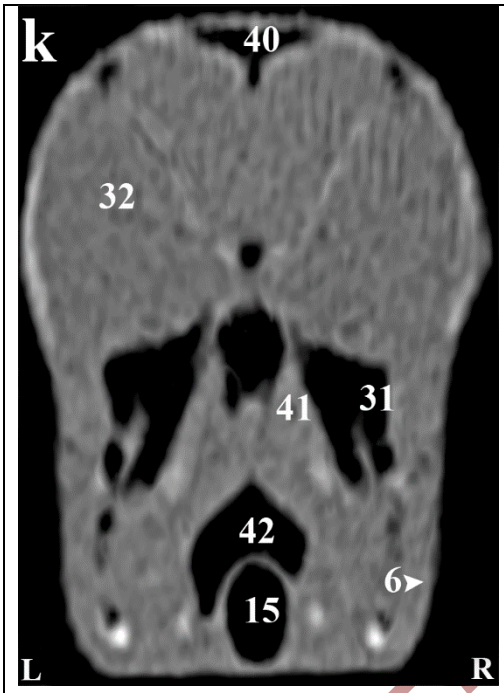

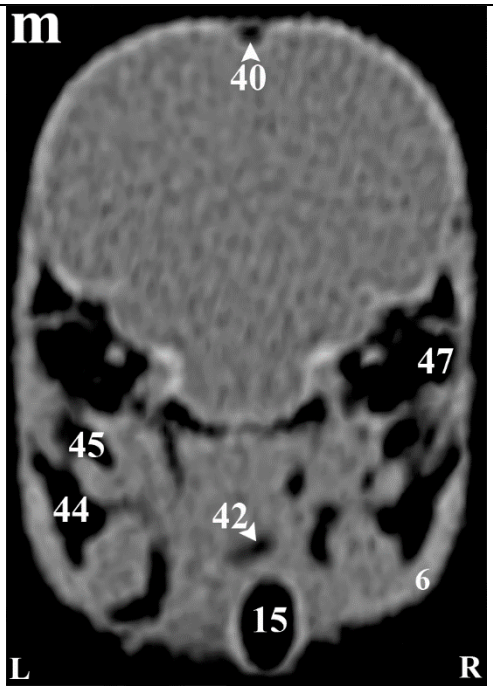

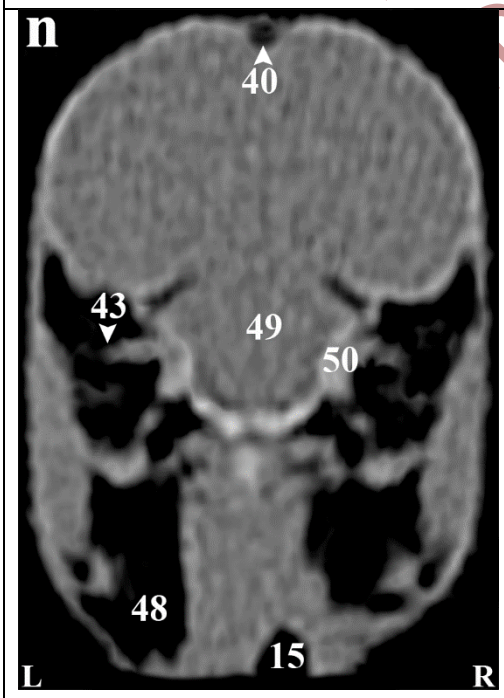

Figure 4. (a-f) Sagittal computed tomography reconstruction images (lateromedial plane) of the normal skull of the cockatiel (*Nymphicus hollandicus*). (1) Scleral bones, (2) Suborbital arch, (3) Postorbital part of the infraorbital sinus, (4) Quadrate bone (pneumonized), (5) External ear foramen, (6) Mandible bone, (7) Cervicocephalic diverticulum, (8) Occipital bones (pneumonized), (9) Infraorbital part of infraorbital sinus, (10) Periorbital process, (11) Epithelial membrane, (12) Jugal portion of infraorbital sinus, (13) Cervical vertebrae, (14) Trachea, (15) Encephalon of the brain, (16) Caudal nasal turbinate, (17) Middle nasal turbinate, (18) Rostral nasal turbinate, (19) Transverse canal, (20) Premaxillary bone (pneumonized), (21) Palate bone (pneumonized), (22) Rostral diverticulum, (23) Frontal bone (pneumonized), (24) Nasal cavity, (25) Nasopharyngeal airway, (26) Larynx, (27) Paraglossum, (28) Basihyal, (29) Bony part of nasal septum, (30) Infraorbital septum, (31) Nostril, (32) Tracheal rings, (33) Cartilaginous part of nasal septum, (34) Tongue. Ca, Caudal; Cr, Cranial.

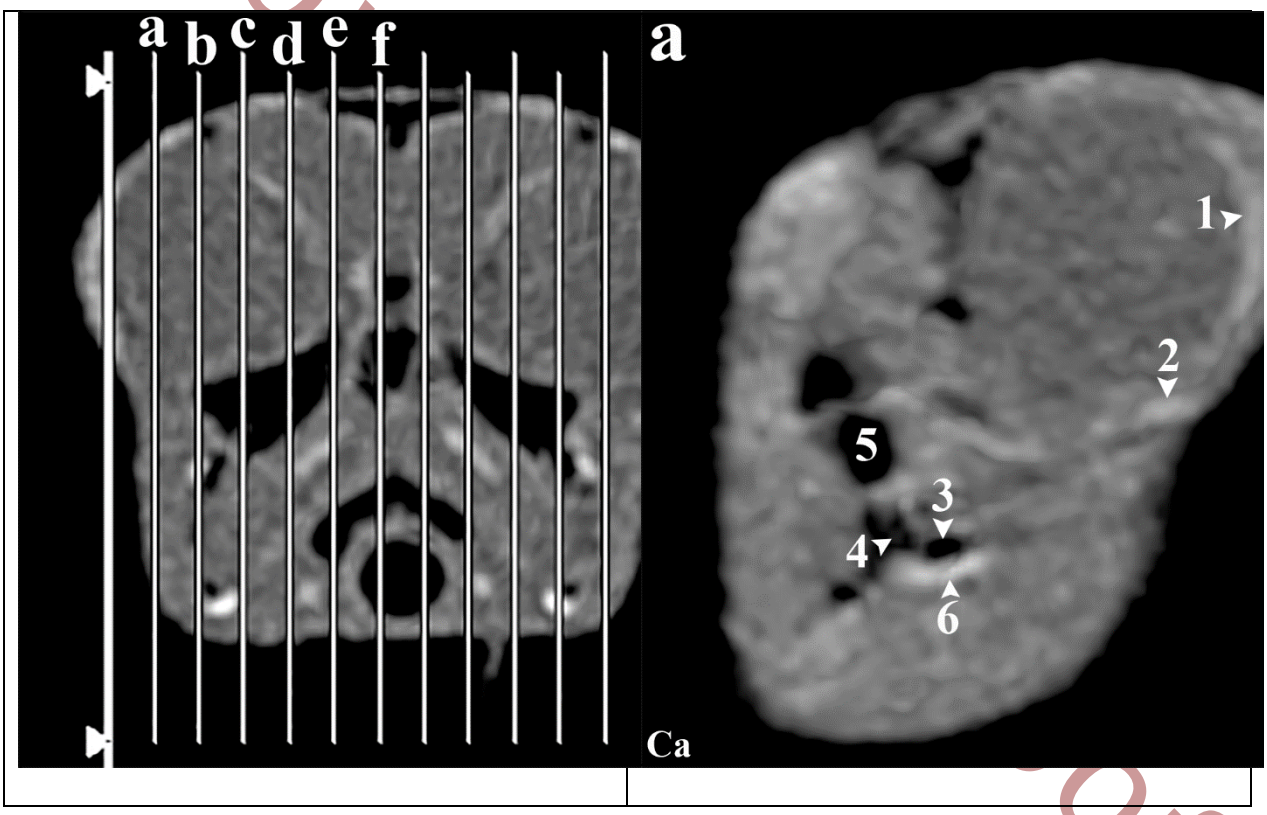

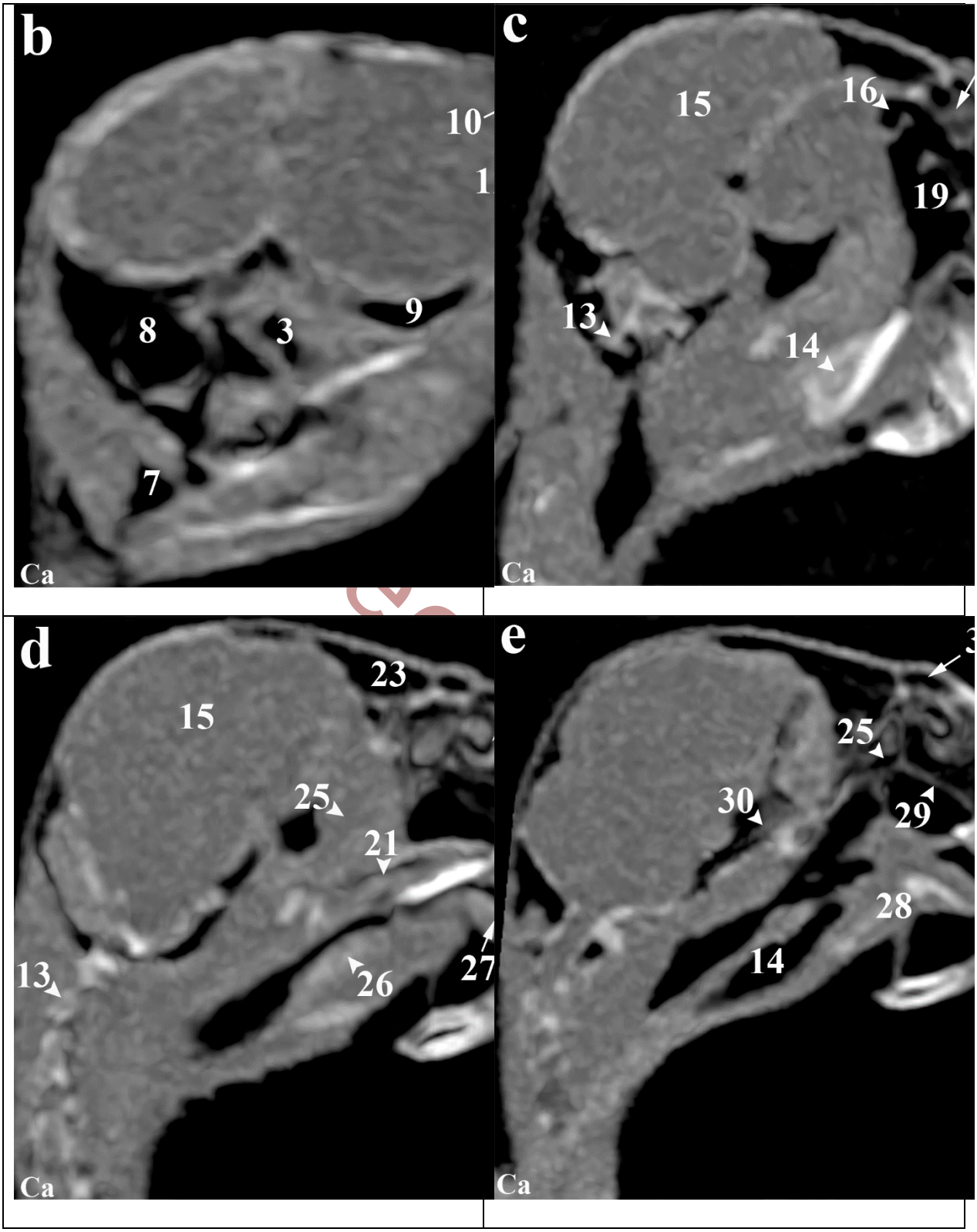
b
10
1
8
3
9
7
Ca
c
15
16
19
13
14
Ca
d
23
15
25
21
13
26
27
Ca
e
25
30
29
28
14
Ca

Figure 5. (a-k) Dorsal computed tomography reconstruction images (ventrodorsal plan) of a normal skull of the cockatiel (*Nymphicus hollandicus*). (1) Basihyal, (2) Arytenoid cartilage, (3) Quadrature part of infraorbital sinus, (4) Epithelial membrane, (5) Quadrate bone, (6) Larynx, (7) Glottis, (8) Pharynx, (9) Pterygoid and quadrate muscle, (10) Mandibular appendage, (11) Oral cavity, (12) External acoustic meatus, (13) Paraglossum, (14) Pterygoid bone, (15) External ear foramen, (16) Bony labyrinth, (17) Jugal arch, (18) Postorbital part of infraorbital sinus, (19) Occipital bones (pneumonized), (20) Suborbital arch, (21) Palate bone, (22) Ethmomandibular muscle, (23) Infraorbital part of the infraorbital sinus, (24) Nasopharyngeal canal, (26) Scleral ossicles, (27) Infraorbital septum, (28) Cartilaginous part of the nasal septum, (29) Palate foramen, (30) Middle nasal turbinate, (31) Rostral diverticulum, (32) Cranial foramen of eyeball, (33) Preorbital part of the infraorbital sinus, (34) Rostral nasal turbinate, (35) Nasal cavity, (36) Bony part of nasal sinus, (37) Infraorbital sinus foramen, (38) Encephalon, (39) Craniofacial flexion, (40) Frontal bone. L, Left; R, Right.

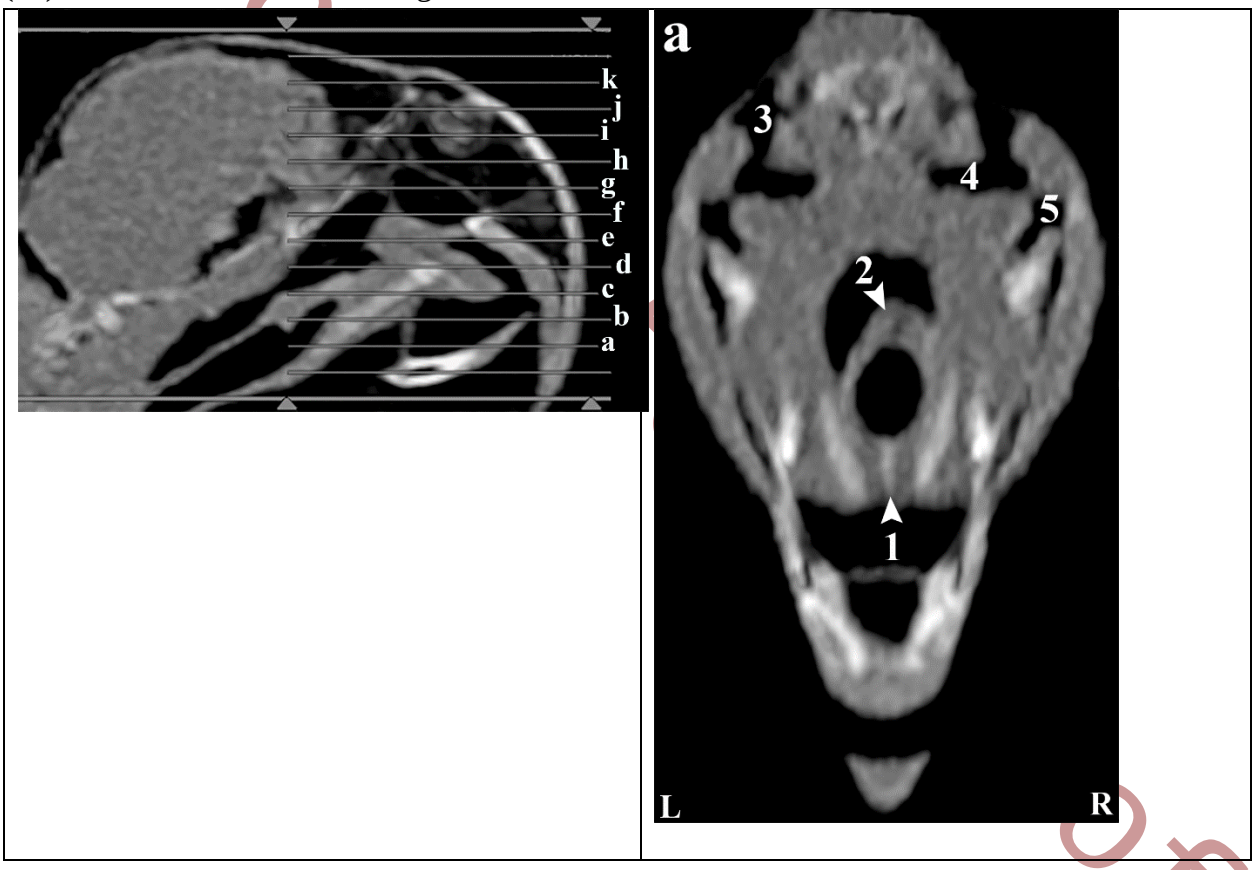

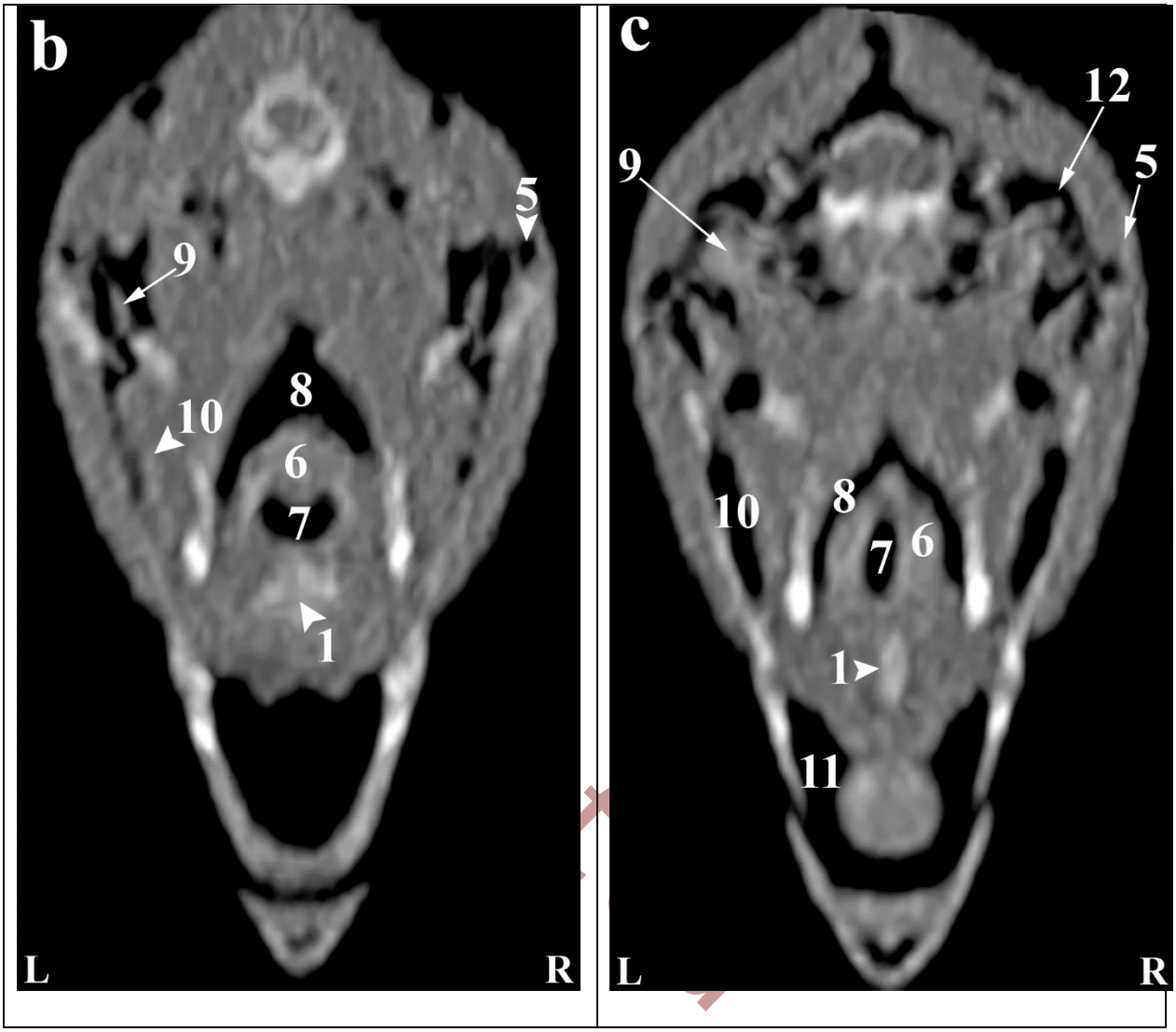

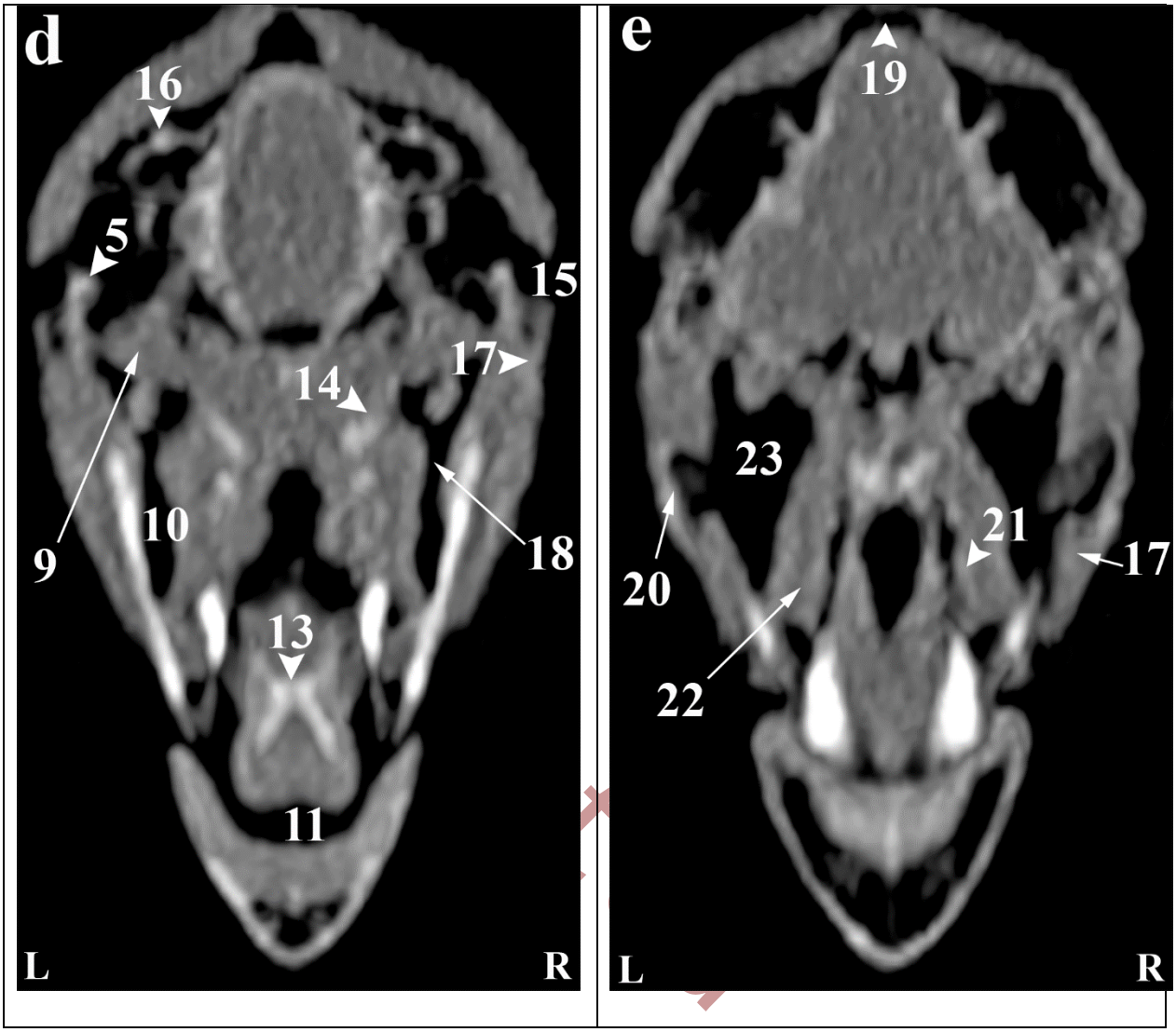

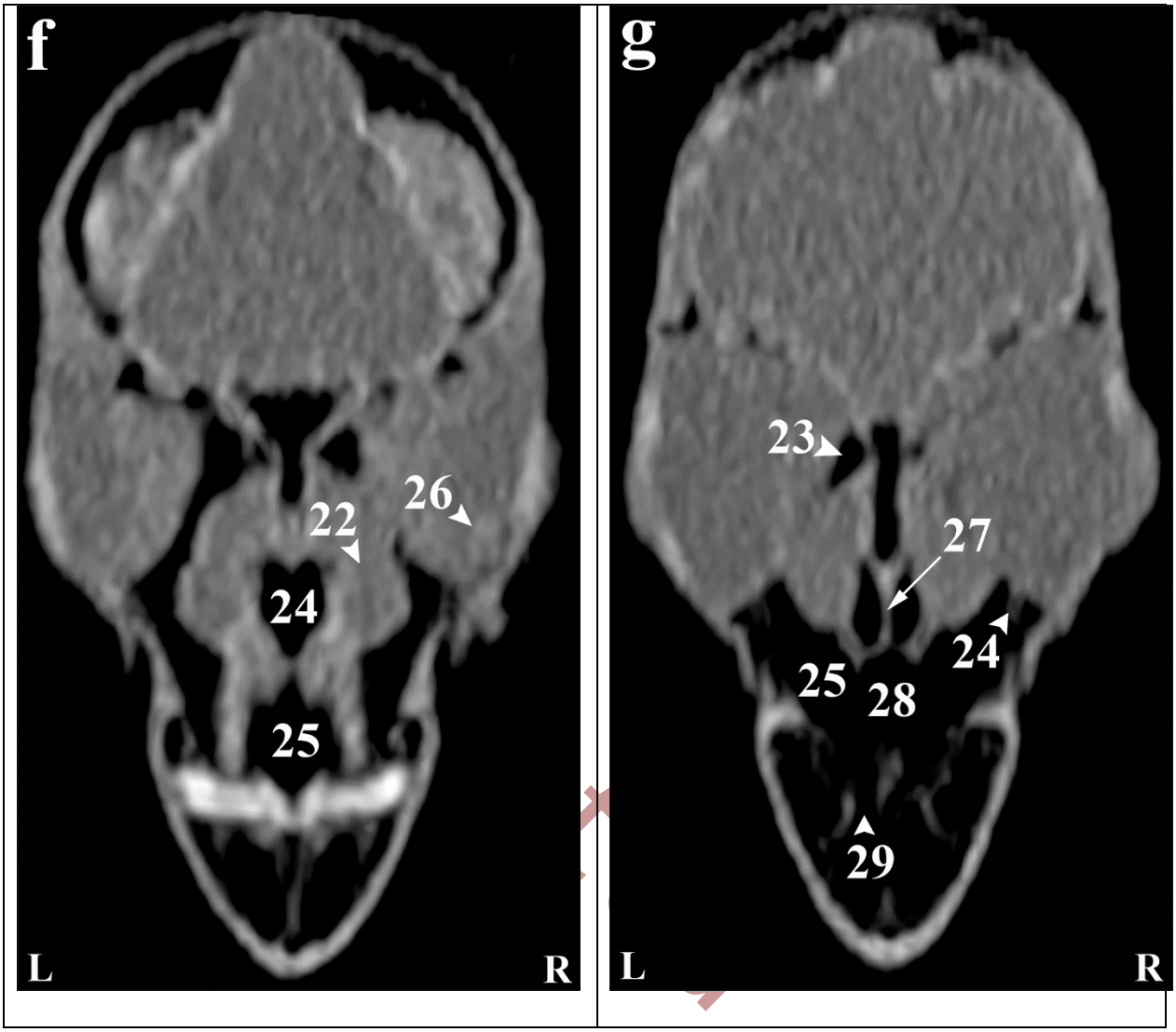

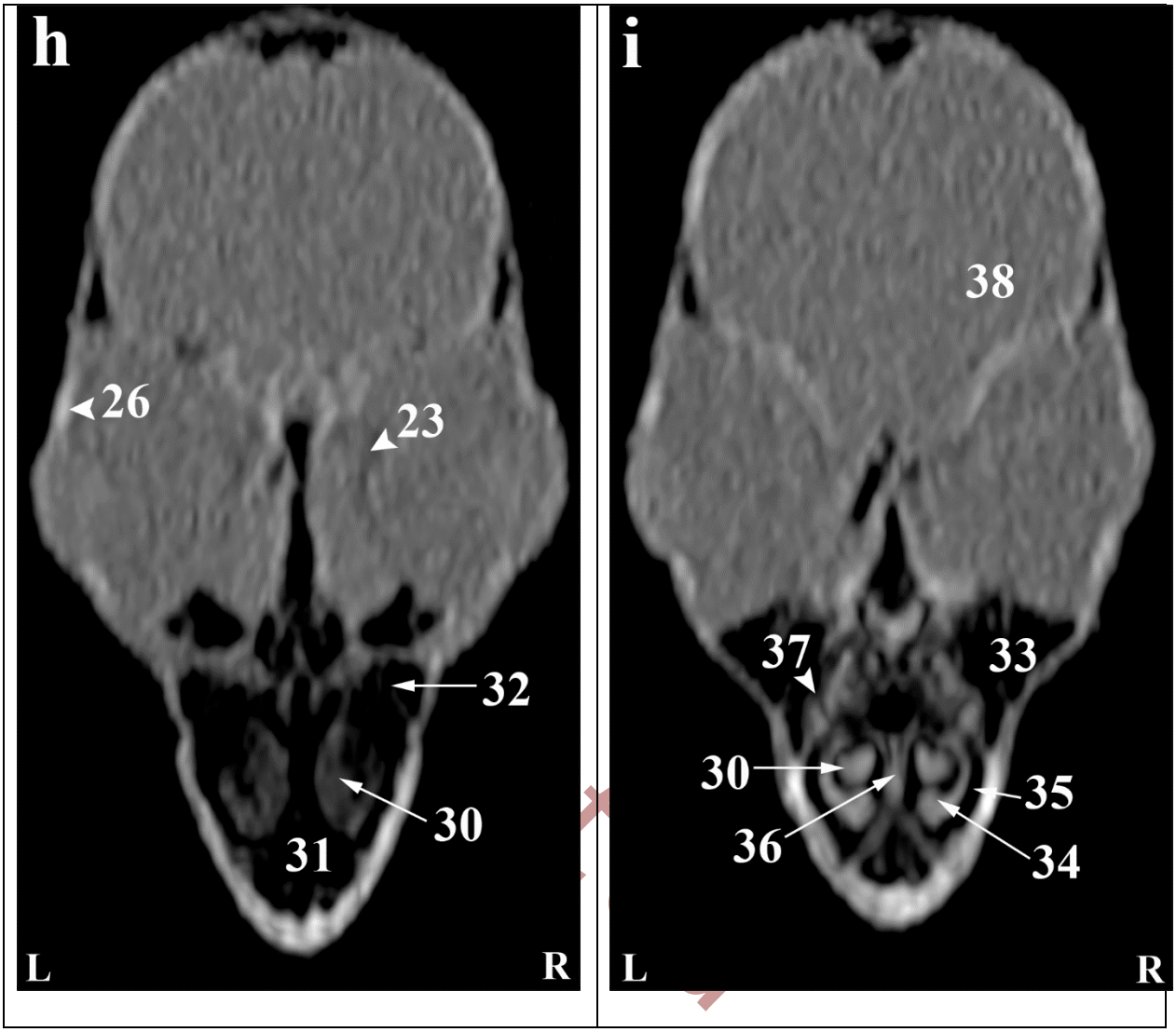

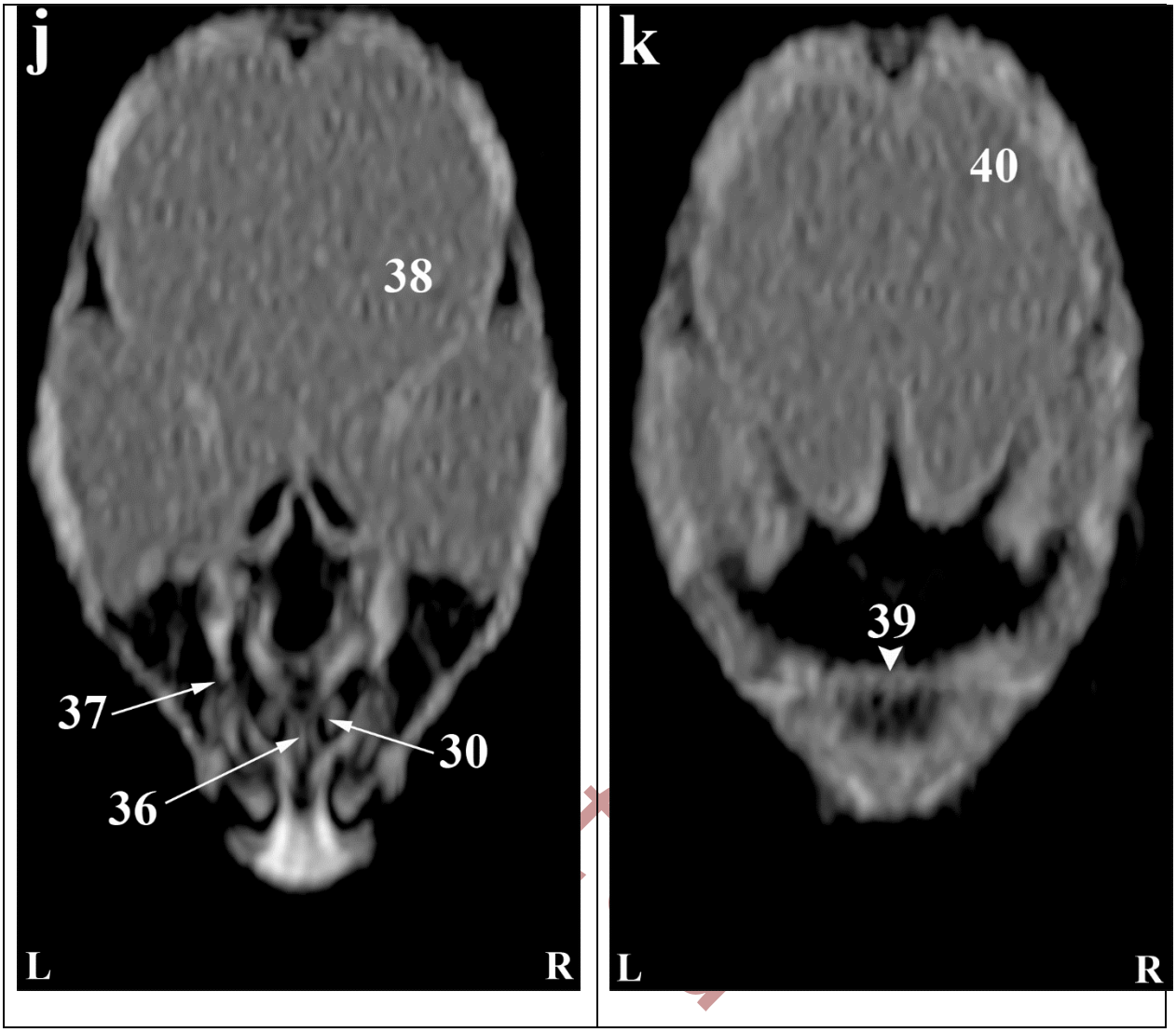

مطالعه رادیوآناتومیکی سر طوطی طوق قرمز (*Psittacula krameri*) بر پایه یافته‌های توموگرافی کامپیوتری

خلاصه

سی‌تی اسکن یکی از کاربردی‌ترین و دقیق‌ترین روش‌های تصویربرداری تشخیصی می‌باشد که می‌تواند برای ارزیابی ناحیه سر در پرندگان استفاده شود. هدف از این مطالعه ارائه اطلاعات آناتومیکی نرمال سر طوطی طوق قرمز (*Psittacula krameri*) به روش توموگرافی کامپیوتری بود. در این تحقیق ویژگی‌های سر این پرنده از نظر استخوان‌ها، مفاصل، عضلات، سینوس‌ها و سایر بافت‌های تشکیل دهنده آن بررسی گردید. در این مطالعه توصیفی - مقطعی از لاشه 6 طوطی طوق قرمز بالغ (3 طوطی نر و 3 طوطی ماده) با میانگین سنی 5-1 سال و با متوسط وزنی 125-115 گرم استفاده شد. پس از تهیه تصاویر توموگرافی کامپیوتری، سر هر طوطی تحت مطالعات آناتومیکی قرار گرفت. بر اساس نتایج این مطالعه اغلب ساختارهای سر طوطی طوق قرمز (*Psittacula krameri*) به وسیله تصاویر توموگرافی کامپیوتری بازسازی شده قابل شناسایی هستند. در تصاویر CT استخوان‌های آهیانه، فک پایین، پس‌سری، ماگزیلاری، پری‌ماگزیلاری، کامی، بالی، چهارگوش، گیجگاهی، غشاهای اپیتلیال، مجرای خارجی گوش و لابیرنت استخوانی، استخوانچه‌های گوش و آنتوگلوسوم، قسمت‌های مختلف سینوس تحت حدقه‌ای، نیم‌کره‌های مغز و قسمت‌های مختلف حدقه چشم و کانکاهای حفرات بینی بررسی گردیدند. مطالعه همزمان ارزیابی توموگرافی کامپیوتری و بررسی آناتومیکی سر طوطی ملنگو همبستگی بالایی از یافته‌ها را فراهم کرد. نتایج این تحقیق می‌تواند در شناسایی خصوصیات آناتومیکی و بررسی گونه‌های مختلف طوطی‌های طوق قرمز (*Psittacula krameri*)، آموزش علوم آناتومی و تفسیر تصاویر CT اسکن و نیز در معاینات بالینی و امور درمانی این نوع از طوطی مورد استفاده قرار گیرد.

کلمات کلیدی: طوطی طوق قرمز (*Psittacula krameri*)، توموگرافی کامپیوتری، آناتومی، سر